Genetic algorithm for optimization of models of the early stages in the visual system

Pablo Martínez-Cañada[a,*], Christian Morillas[a], Hans E. Plesser[b], Samuel Romero[a], Francisco Pelayo[a]

[a] *CITIC, Department of Computer Architecture and Technology, University of Granada, Spain*
[b] *Department of Mathematical Sciences and Technology, Norwegian University of Life Sciences, Norway*

Abstract

Automated parameter search methods are commonly used to optimize neuron models. A more challenging task is to fit models of neural systems since the model response is determined by both intrinsic properties of neurons and the neural wiring and architecture of the network. Neural records of cells in the visual system are often analyzed in terms of the cell's receptive field and its temporal response. This type of data requires a finer point-by-point comparison of response traces between the simulated output and the recorded data. To address these issues, we applied a genetic algorithm optimization in conjunction with a multiobjective fitness function and a population-based error metric. Two different models of the early stages in the visual system were fitted to electrophysiological recordings and results from a modeling study, respectively. The first one is a model of cone photoreceptors and horizontal cells that reproduces adaptation to the mean light intensity in the retina. A multiobjective fitness function based on the normalized root-mean-square error (NRMSE) and a shape error descriptor captures high-frequency oscillations in the impulse response to uniform white flashes. The second one is a large-scale model of the thalamocortical system that accounts for the slow rhythms observed during sleep. An error

*Corresponding author
Email addresses: pablomc@ugr.es (Pablo Martínez-Cañada), cmg@ugr.es (Christian Morillas), hans.ekkehard.plesser@nmbu.no (Hans E. Plesser), sromero@ugr.es (Samuel Romero), fpelayo@ugr.es (Francisco Pelayo)

metric of the population neural activity is used in this case. We argue that the optimization framework proposed in this paper could serve as a useful tool for parameter fitting of neuron models and large-scale models in the visual system pathway.

Keywords: Genetic algorithm, multiobjective parameter fitting, neural system optimization, retina model, thalamocortical system

---

1. Introduction

Neuron models often have many parameters that are difficult to estimate manually. Parameter optimization is facilitated by automated search methods that minimize an error metric representing differences between simulated and experimental data[1, 2, 3, 4, 5, 6]. Traditionally, models of the early visual pathways, referred to the retina, Lateral Geniculate Nucleus (LGN) and primary visual cortex (V1), are either hand-tuned, using a trial-and-error method, or defined in terms of the well-known linear-nonlinear (LN) modeling[7, 8, 9, 10, 11, 12, 13, 14, 15, 16]. Although some of the model parameters are constrained experimentally, yet some of them cannot be measured by simple electrophysiological methods, especially when the model is complex and its response described by a large number of parameters. We can also find other models whose parameters are tuned by an optimization algorithm[17, 18, 19, 20, 21, 22, 23]. In the retina model proposed by Ozuysal and Baccus[19], multiple initial points are used by a nonlinear programming solver to converge to different local optima and then choose the best solution. Besides, a function that computes the error of the estimated membrane potential across the time and frequency domains allows capturing both slow shifts in potential and high-frequency fluctuations. Mante et al.[20] optimized independently each stage of their LGN model in a multi-step fitting process based on the mean-squared error (MSE). In the photoreceptor model by van Hateren[22], the parameter fitting is based on linear programming for minimizing the root-mean-square deviation (RMSD) between model responses and measurements. In simultaneous-response fitting,

the RMSD of the highest responses are multiplied by a scaling factor to prevent biased results.

A genetic algorithm (GA)[24] is a popular, biologically inspired optimization method that can prevent the search from converging on local minima. In addition, GAs do not need a differentiable mathematical expression, or an estimate, of the objective function, like in gradient methods. Therefore, GAs are more likely to find the global optimum, and require relatively little knowledge of the problem being solved. Although the computation of the fitness function can be time-consuming, the inherently parallel nature of GAs simplifies the implementation of a multiprocessing architecture. In this paper, a GA optimization is shown to be an effective solution that facilitates parameter search of neural models with a minimal configuration setup.

The second critical component of the optimization algorithm is the error metric. We can distinguish three types of error metrics commonly used in neuron model optimization: feature-based, point-by-point comparison of response traces and multi-objective functions[1]. In experiments that study the visual processing pathway, neurons are often stimulated by synthetic input patterns (e.g., sinusoidal drifting gratings) and their neural outputs characterized by changes produced in their receptive fields and temporal responses[25, 26, 27, 28]. Fitting every feature of this type of responses is crucial to understand the mechanisms involved in the visual function and, as discussed in Section 2.2, a standard point-by-point comparison of traces (e.g., by using only the MSE) is insufficient to characterize high-frequency components of the neural signal. Here, we describe a multiobjective fitness function that combines two types of error metrics, the normalized root-mean-square error (NRMSE) and a shape error descriptor. Our approach captures high-frequency oscillations of the temporal response and overcomes also the problem of rescaling the data to prevent biased results.

Parameters of the large-scale model of the thalamocortical system were fitted by a feature-based error metric that compares the average membrane potential of the population in specific time intervals. We used the target membrane potentials estimated from results of the modeling study of this system. The GA

optimization allowed us to bring the model of the thalamocortical system into a stable parameter regime where it reproduces qualitatively the neural behavior of the original model.

2. Methods

2.1. Genetic algorithm optimization

Genetic algorithms have shown to be an effective method for constraining conductance-based compartmental models[2, 3, 29]. In our implementation, an individual of the population of candidate solutions is an array of real numbers that represent parameters of the simulation model to be optimized. These parameters are constrained to be within a biological range (e.g., time constants are between 1 and 100 ms). We use two different selection operators, tournament selection for single-objective optimization, which has several benefits over alternative selection methods[30], and one of the most commonly used Pareto optimization algorithm, NSGA-II[31]. The genetic operator selected for crossover is uniform crossover. Different operators were tested (such as one-point and two-point crossover algorithms) but we found no difference in results, only in the convergence speed of the genetic algorithm. Similarly, in the chosen Gaussian mutation operator, different values of μ and σ were evaluated, observing some slight differences in the convergence rate. The genetic algorithm is implemented by using the Python library DEAP[32].

Evaluation of the fitness function for each individual represents the bottleneck in the processing of the genetic algorithm. Computation of the fitness function in the thalamocortical system model can take up to 180 s using an Intel Core i7-3630QM CPU. In this model, when 512 individuals are evaluated along 100 generations (51200 evaluations in total), the GA optimization is completed after 2560 hours using a single processor. In order to overcome this drawback, we implemented a parallel processing architecture in a computer cluster based on the MPI interface[33] that distributes evaluation of individuals across different processes. Thus, the fitness functions of 512 individuals are computed

in parallel, with 512 processes running in 512 CPUs, and the GA is executed within 5 hours.

Distributed computing allows the use of multiple computers simultaneously and enables larger simulations. When computing the fitness function, memory usage of our simulations can increase up to 1.8 GB as a result of the storage of membrane potential values of each cell for every millisecond of simulation. The maximum memory per CPU provided by the cluster used in this work, the supercomputer Alhambra of the University of Granada[34], is 1.8 GB. We thus chose an MPI distributed-memory parallelization that maps every process to one CPU and fully exploits all resources of every computation node. In particular, we use the MPI specification included in the Python library *mpi4py*[35]. In other experiments, with a larger memory cluster (not reported here), this parallelization scheme was combined with thread-parallel simulation in every node. This hybrid architecture was implemented by enabling the option of OpenMP[36] thread-parallelism provided in NEST. With this configuration, every process executes faster simulations in NEST using multiple threads.

To distribute evaluation of the fitness function to the different computation nodes we used a well-known master-slave configuration whereby a root process evenly splits the population array every generation and scatters data to the rest of processes. The population size was a multiple of the number of processes in such a way that every process receives the same number of individuals and the computing load, therefore, is balanced in the network. All processes then compute in parallel the fitness functions of the assigned individuals. Once all individuals are evaluated, the root node gathers individual fitnesses from all processes and resumes the evolutionary algorithm.

2.2. Error metrics and fitness functions

2.2.1. Multiobjective optimization

When comparing point-by-point voltage traces of the simulated model response and target data, a mere MSE-based metric may provide misleading results (as illustrated in the example of Fig. 1). In this figure, the temporal

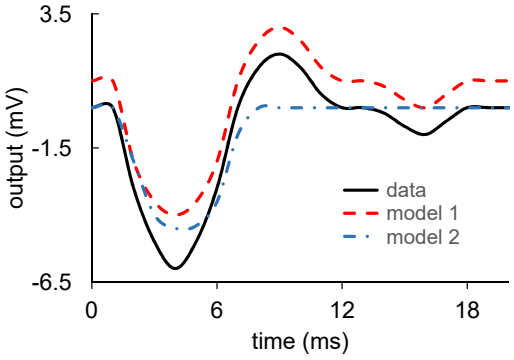

Figure 1: Example that illustrates the voltage traces generated by two arbitrary models attempting to approximate the measured data.

response of a fictional neuron is generated (labeled as *data*) and compared with the temporal responses of two different models (*model 1* and *model 2*), handmade as well. An MSE-based metric (NRMSE) and a shape error descriptor, detailed below, are computed between data and model responses, shown in Table 1. Although the voltage trace of *model 1* reproduces better the target oscillatory behavior, its NRMSE is higher when compared with *model 2* because of an offset difference. It is, therefore, necessary to add a second metric that considers also the shape of responses, where the information of high-frequency components lies. In other fields, as in hyperspectral imaging, the joint effect of these two types of metrics has been also employed to accurately compare spectral data in terms of shape and offset[37, 38].

We define the NRMSE as:

$$NRMSE = \frac{\sqrt{\sum_i (data_i - model_i)^2 / n}}{data_{max} - data_{min}} \tag{1}$$

The error is computed between n samples of target data ($data_i$) and model response ($model_i$), and normalized within the data range ($data_{max} - data_{min}$). Error normalization to the data range prevents biased results in simultaneous-response fitting for different input stimuli.

Table 1: NRMSEs and shape errors obtained for models in Fig. 1.

	model 1	**model 2**
NRMSE	0.1404	0.1104
Shape error	0.0114	0.1487

We also introduce a shape error metric that is calculated by averaging angular differences between line segments that connect target and model samples:

$$shape_{error} = \min_{s} \left(\frac{\sum_i \left(arccosine \left(\frac{\vec{a_i} \cdot \vec{b_{i,s}}}{\|\vec{a_i}\| \|\vec{b_{i,s}}\|} \right) / \pi \right)}{n-1} \right) \tag{2}$$

every line segment i connecting data samples is defined as a vector $\vec{a_i}$ wherein coordinates along the x-axis refer to the time (or spatial) axis, and along the y-axis to the target response: $\vec{a_i} = (t_{i+1} - t_i, data_{i+1} - data_i)$. Similarly, the y-axis of the vector $\vec{b_{i,s}}$ is referred to the model response: $\vec{b_{i,s}} = (t_{i+1+s} - t_{i+s}, model_{i+1+s} - model_{i+s})$. Since an exact shape matching of model and data responses may be considerably difficult to achieve, a more flexible approach is selected so that we allow a small shift of the traces in the x-axis by s positions when computing the error. The minimum error for all shifts is selected as the final shape error. A shift of ± 1 was fixed for our simulations. We apply this metric to monotonically increasing functions, e.g., temporal series and spatial responses, so that the *arccosine* is always positive within the range $[0, \pi]$ and, thus, the shape error is normalized as well.

These two metrics are integrated into the multiobjective optimization algorithm as follows: given that there are M responses to optimize simultaneously, corresponding to k different input stimuli, the two fitness functions are simply formulated as average sums of the NRMSE and shape errors, respectively, for all responses:

$$fitness_{multobj1} = \sum_k (NRMSE_k)/M \tag{3}$$

$$fitness_{multobj2} = \sum_{k}(Shape_k)/M \tag{4}$$

2.2.2. Single-objective optimization

On the other hand, parameters of the large-scale model of the thalamocortical system were fitted by a feature-based error metric that compares the average neural responses of the population in specific time intervals. Our goal for this model was to bring it into a stable parameter regime where it reproduces qualitatively the simulation results of the original publication. We found that a single-objective optimization is sufficient to fit the target membrane potentials estimated from the original study.

The following fitness function computes the RMSE between the average membrane potential of the simulated population in a time interval t, $V_{sim}(t)$, and the target average membrane potential, $V_{tar}(t)$:

$$fitness_{singobj} = \frac{\sum_l \sqrt{\sum_t (V_{tar}(t) - V_{sim}(t))^2/T}}{L} \tag{5}$$

where T is the total number of time intervals. For a multi-layered model, responses of L neural layers (from $l = 1$ to L) are optimized simultaneously by averaging as well this error across them. We approximated the oscillatory behavior of this model during sleep by simply using the average membrane potential of the population. Nevertheless, different feature-based error metrics (e.g., after-hyperpolarizing potential or firing rate[1, 2]) can be easily embedded in our single-objective optimization scheme to consider other properties that may be more discriminative depending on the target data.

2.3. Models of the early stages in the visual system

The above-described optimization framework was applied to models of the retina cones and horizontal cells and the thalamocortical system (shown in Fig. 2). The first model was implemented using COREM[39, 40, 41], a software platform that provides a set of computational retinal microcircuits that

can be used as basic building blocks for the modeling of different retina mechanisms. We simplified and adapted the molecular model of cones and horizontal cells proposed by van Hateren[22] to fit electrophysiological data obtained from horizontal cells of the macaque retina[27]. There are 22 parameters distributed across the three principal stages of the model: outer segment (phototransduction and calcium feedback), inner segment and horizontal cell's feedback mechanism. In Fig. 2A, $L_{n,\tau}(t)$ represents a temporal linear filter, SNL is a static nonlinearity and $C_m dV(t)/dt$ a single-compartment model. Two parameters define the temporal linear filter: the time constant τ and the number of low-pass filtering stages, n. The static nonlinearities of the outer and inner segments are polynomial functions with slope a, exponent b and offset c. The static nonlinearity of the horizontal cell feedback is a sigmoidal function described by the following equation: $y(x) = b/(1 + exp(-ax + c))$. C_{calc} and C_{inner} are cell's membrane capacitances of the single-compartment models.

Photoreceptors' neural response to uniform white flashes of different time length was recorded at a fixed Weber contrast of 8 and varying background illuminance. The model fittings were made to nine stimulus conditions simultaneously (resulting from all possible combinations of three different time lengths and three background light intensities), which means a value of $M = 9$ in Eqs. 3 and 4. We applied the multiobjective optimization approach to fit a target set of temporal impulse responses. Further details on the model are provided in reference [39].

The second model is an implementation of the thalamocortical system developed by Hill and Tononi[42] using NEST 2.8.0[43]. This is a large-scale model that encompasses portions of two cortical visual areas and associated thalamic and reticular thalamic nuclei, with thousands of model neurons that incorporate both intrinsic and synaptic currents. It accounts for the transition from wakefulness to sleep and the generation of the slow oscillation. We decided to maintain the same network configuration (e.g., synaptic masks, kernels and weights) as in the original model so that only peak conductances of intrinsic ion channels are optimized, allowing to countervail slight deviations in the model

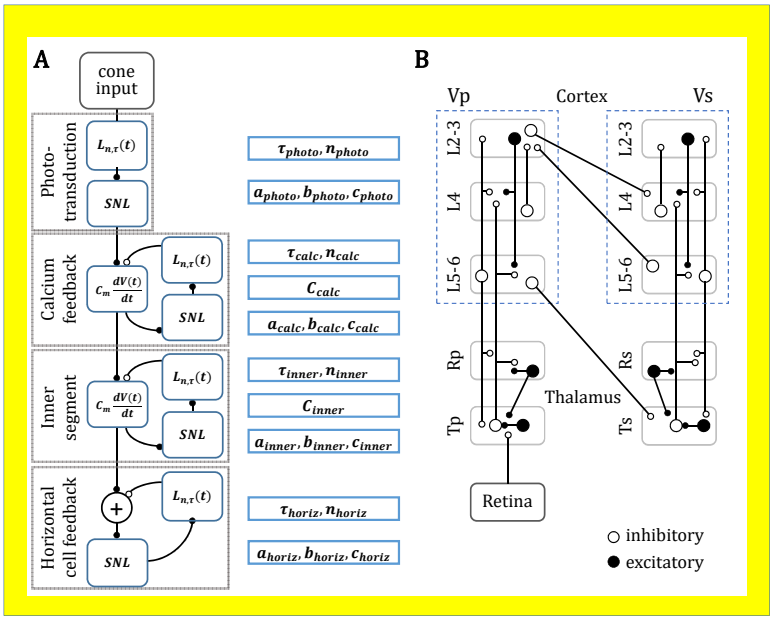

Figure 2: Schematic of the two models. A: Model of the retina cones and horizontal cells including parameters to be optimized for each stage (Figure adapted from [39]). B: Thalamocortical system with its main interlaminar and interareal connections, as well as thalamocortical and corticothalamic connections (Figure adapted from [42]). The primary visual area includes a 3-layered cortical area (Vp), reticular nucleus (Rp) and dorsal thalamus (Tp). The secondary visual area is formed by its associated cortical area (Vs), reticular nucleus (Rs) and dorsal thalamus (Ts).

output as a result of using different simulators. We studied how the increase in the potassium leak conductance and the four intrinsic conductances can drive the transition from the waking mode to the sleep mode. This transition is simulated in two time-discrete steps: initial peak conductances are first set to half of their values for the waking mode, temporal simulation advances for 400 ms and then these peak values are set to the final values maintained during the waking mode. Therefore, there is a total of 10 parameters to optimize: initial and end peak conductance values. For this purpose, we applied the single-objective optimization to fit the average membrane potential of the different neural layers.

The model neuron of the thalamocortical system is a single-compartment

spiking neuron incorporating Hodgkin-Huxley currents:

$$I_{channel} = g_{peak} m^N h (V - E_{channel}) \tag{6}$$

where g_{peak} is the maximal conductance of the channel, m and h determine its activation and inactivation respectively, V is the membrane potential and $E_{channel}$ is the reversal potential for the given channel. The factor N allows the activation to occur in a different order than inactivation. Optimization is conducted on the following intrinsic channels: persistent sodium current ($I_{Na(p)}$), pacemaker current (I_h), low-threshold calcium current (I_T) and depolarization-activated potassium current (I_{DK}), in addition to the potassium leak conductance (see reference [42] for further details on these conductances).

3. Results

3.1. Model of the retina cones and horizontal cells

We experimented with different combinations of the following GA parameters: number of generations, population size, crossover and mutation rates. In Fig. 3, we plot optimization results when the GA is configured with 200 generations, 800 individuals in the population and crossover and mutation rates of 0.5 and 0.3, respectively. Under other conditions, the GA never converges (both hyperparameters greater than 0.5) or its convergence rate is lower and the algorithm does not find an optimal solution within 200 generations (crossover and mutation rates below than 0.1). We compute the hypervolume as the area of the 2-dimensional space contained by the solutions to the Pareto-optimal front and a reference point. Evolution of the hypervolume shows that approximately after 50 generations the GA converges to an optimal solution. However, a slightly better tune of model parameters is found when the hypervolume rises again after 160 generations, decreasing to a greater extent the shape error.

Two extreme solutions of the Pareto front are also shown as an example of results reached by emphasizing one or the other error metric. High-frequency oscillations are better captured by the solution depicted at the bottom of the

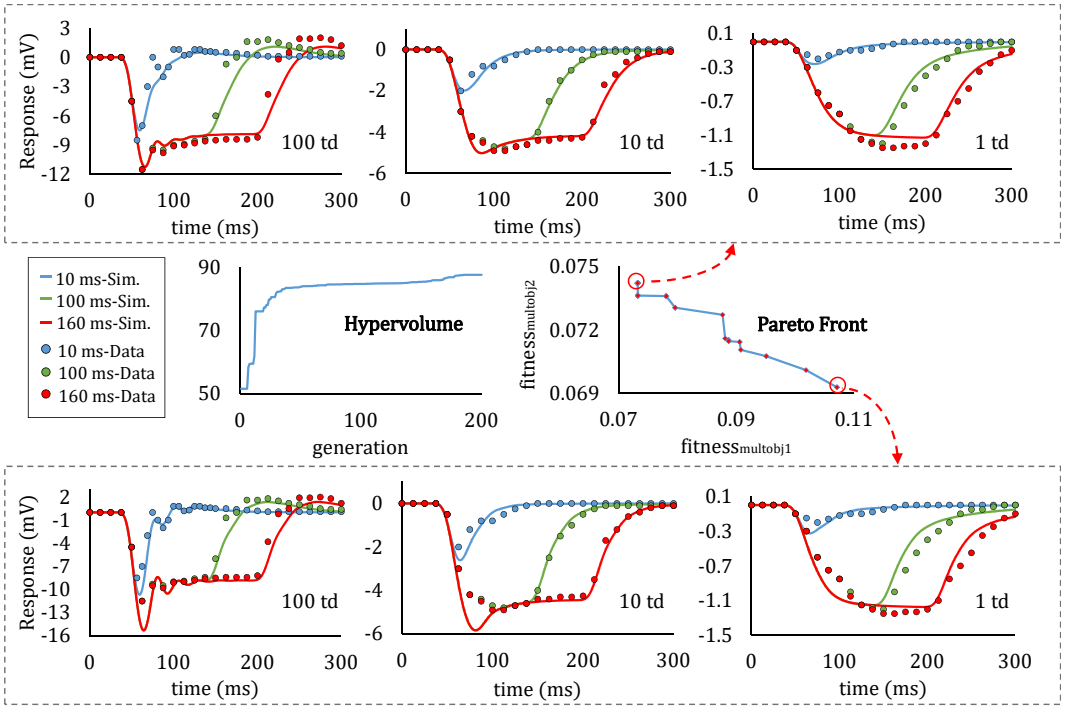

Figure 3: Results of the multiobjective optimization applied to the model of the retina cones and horizontal cells. Evolution of the hypervolume over generations and the estimated Pareto front are shown in the center of the figure. Two extreme solutions of the Pareto front are depicted at the top (minimum NRMSE) and bottom (minimum shape error). They represent simulation results of the model (color solid lines) and electrophysiological recordings (color markers) obtained from horizontal cells of the macaque retina[27]. Data points have been sampled from Figure 6 in the publication[27]. Input stimuli are spatially uniform white flashes of 10, 100, and 160 ms at a fixed Weber contrast of 8 and background illuminances of 100, 10 and 1 trolands (td). All flashes start at 0 ms.

figure, where the shape error is minimum, particularly within the first 100 ms of the 100 td response. However, this solution presents also significant offset errors in some specific points (observe the minimum value of the 100 and 10 td responses). On the other hand, the solution at the top of the figure limits this high-frequency behavior but the squared-error is minimized for all samples.

Table 2: Parameters of the two extreme solutions in the Pareto front according to Fig. 3. The different stages of the model are Phototransduction (Photo.), Calcium feedback (Calc. F.), Inner segment (Inner S.) and Horizontal cell feedback (Hor. F.). Time constants (τ) are specified in milliseconds and the rest of parameters are unitless. C_{calc} and C_{inner} are both 1.0 $\mu F/cm^2$

	Minimum shape error					**Minimum NRMSE**				
	τ	n	a	b	c	τ	n	a	b	c
Photo.	40.0	4.1	-0.4	1.0	5.2	40.0	4.1	-0.4	1.0	5.2
Calc. F.	44.4	0.9	6.4	4.0	-3.6	44.4	0.8	6.4	4.0	-3.6
Inner S.	79.9	3.3	22.4	2.0	8.3	79.9	3.3	22.4	2.0	8.3
Hor. F.	12.5	1.5	182.2	71.0	2.8	9.9	1.5	182.2	71.0	2.8

The different parameter sets of these two solutions are shown in Table 2.Only the number of low-pass filtering stages (n) of the calcium feedback and the time constant (τ) of the horizontal cell feedback differ between the two solutions. However, we observed that the high-frequency oscillatory behavior of the retinal response is mainly determined by the latter parameter (τ), even for variations of less than 3 ms. Intermediate solutions provide a trade-off between these two error functions.

3.2. Thalamocortical system

In this model, the transition from the waking mode to the sleep mode (see Fig. 4) comes about by increasing the potassium leak conductance and the four intrinsic conductances. The single-objective fitness function (Eq. 5) averages the error across the 5 populations shown in Fig. 4 A and the following 5 time intervals: wakefulness (from 0 to 200 ms), transition to the sleep mode (from 200 to 600 ms), first oscillation of the sleep mode (from 600 to 1100 ms), downstate (from 1100 ms to 1600 ms) and second oscillation (from 1600 to 2100 ms). During the first time interval, peak conductances are set to an initial value (g_I) and afterward, in the second time interval, they are modified to half of their maximum values in the sleep mode. From the third time interval on,

Table 3: Target average membrane potentials (mV) used in the optimization according to reference [42].

	L2-3	**L4**	**L5-6**	**Rp**	**Tp**
0-200 ms	-65	-65	-65	-68	-68
200-600 ms	-75	-75	-75	-70	-70
600-1100 ms	-58	-58	-58	-65	-68
1100-1600 ms	-75	-75	-75	-75	-75
1600-2100 ms	-58	-58	-58	-65	-68

conductances take their maximum value (g_E). Although conductances were fitted only to the first 2100 ms, the model remains stable afterward for an extended period of time showing that the fit is reasonably robust.

We used the target average membrane potentials shown in Table 3. Average membrane potentials of the up- and down-states of the cortical layers are -58 and -75 mV respectively, according to values provided in reference [42]. Other values are interpolated by visual inspection of results published by Hill and Tononi[42].

The GA is configured with 100 generations, 512 individuals in the population and crossover and mutation rates of 0.5 and 0.3, respectively. Optimal peak conductances are: potassium leak conductance g_{KL}, between 1.0 (initial value) and 2.2 (end value); persistent sodium current $I_{Na(p)}$, 1.0 and 5.0; pacemaker current I_h, 0.01 and 4.61; low-threshold calcium current I_T, 0.97 and 2.07; and depolarization-activated potassium current I_{DK}, 0.17 and 2.27.

With the increase in the potassium leak conductance (its peak value goes from 1.0 to 2.2) the network enters the hyperpolarized state of around -75 mV. The 3 primary active intrinsic currents underlying the up- and down-states in cortical neurons are I_h, $I_{Na(p)}$ and I_{DK}, as shown in Fig. 5. These 3 currents experience a significant increase during the sleep mode compared to the waking mode. I_h is hyperpolarization-activated, shifting the membrane potential towards a more depolarized level during the down-state. When the membrane

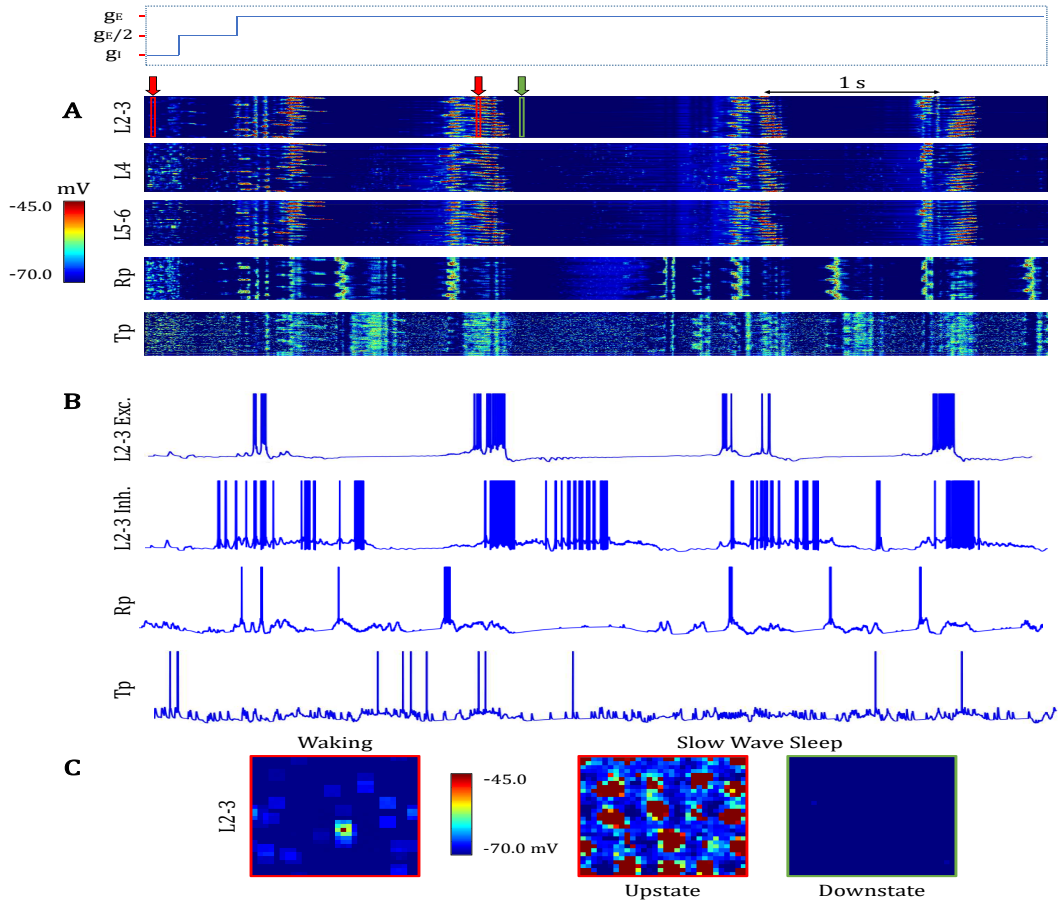

Figure 4: Simulation of the transition from the waking mode to the sleep mode in the thalamocortical visual system (see Fig. 4 in the reference publication[42]) with the optimal set of parameters found by the single-objective optimization. g_I and g_E are the initial and end values of intrinsic conductances. A: membrane potential rasters of 100 neighboring cells in the primary visual area over 5.1 s (cortical layers L2-3, L4 and L5-6, and reticular nucleus cells (Rp) and thalamocortical neurons (Tp)). B: membrane potential traces from excitatory and inhibitory cells in cortical layer L2-3, Rp and Tp. C: topographical activity plots show the average membrane potential during wakefulness (green), and the upstate and downstate of the slow oscillations in the sleep mode (green and red). Red and green boxes (in A) during the waking mode and the sleep mode indicate the time window (10 ms) of the averaged activity.

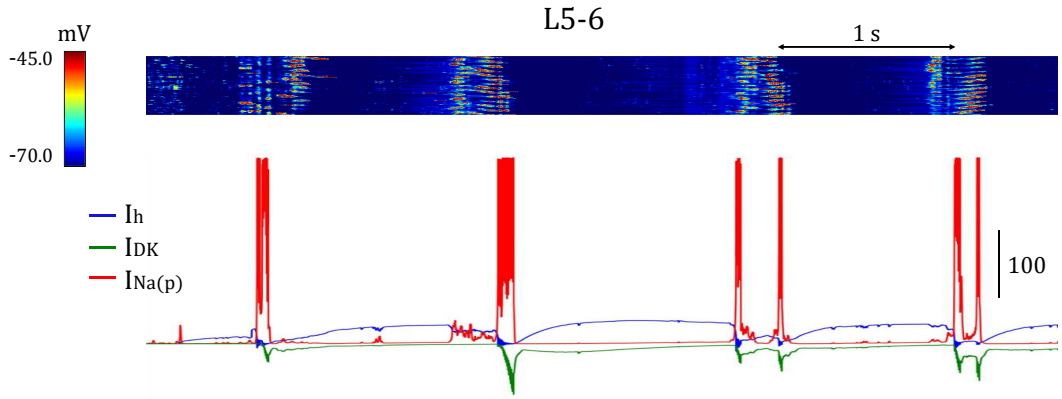

Figure 5: Membrane potential raster of cortical layer L5-6 compared with the individual intrinsic current traces for a selected cell in this layer. Conductance units are dimensionless since the neuron model does not have a defined area or volume.

potential exceeds a certain threshold, $I_{Na(p)}$ activates, promoting a spike burst. This burst initiates the depolarized phase of the slow oscillation until I_{DK}, also activated during spiking, progressively forces the cell to enter again the hyperpolarized state. The interplay among $I_{Na(p)}$, I_{DK} and I_h during sleep is determinant for shaping oscillations of the slow wave. I_T, only present in thalamus cells, does not increase significantly during the sleep mode (results not shown here), what discards a key role of this current.

4. Discussion

Numerous approaches have been proposed to automatically search for sets of parameters of neuron models that best fit available experimental data[1, 2, 44]. The response of a neural system, however, is described by both intrinsic parameters that define the cells' morphology and biophysical dynamics and parameters of the network architecture and connections. We employed a genetic algorithm optimization, implemented with the Python library DEAP[32], to fit parameters of two different models of the visual system. The first one is a

model of cone photoreceptors and horizontal cells that reproduces adaptation to the mean light intensity in the retina. It was configured using the simulation platform COREM[39]. The second model is an implementation of the large-scale thalamocortical system developed by Hill and Tononi[42] using NEST 2.8.0[43].

In the electrophysiology of the visual system, fitting every feature of the neuron's receptive field or the temporal response to specific stimulus conditions, is crucial to understand the mechanisms involved in the visual function. We have shown that a standard point-by-point comparison of response traces (e.g., by using only the MSE) is insufficient to accurately compare data and model responses. A multiobjective error metric has been proposed based on a combination of the normalized root-mean-square error (NRMSE) and a shape error descriptor. We used this metric in conjunction with the well-known algorithm NSGA-II[31] to search for parameters of the model of cone photoreceptors and horizontal cells. Secondly, parameters of the model of the thalamocortical system are fitted by a single-objective feature-based error function. This function computes differences between data and model responses in terms of the average membrane potential of a set of neuron populations in specific time intervals.

Two extreme solutions of the multiobjective optimization have been used in Fig. 3 as an example of the type of results reached by giving more weighting to the NRMSE or to the shape error. High-frequency oscillations are better captured by the minimum shape-error solution of the Pareto front, particularly within the first 100 ms of the 100 td response. However, this solution presents also significant deviations from the target data in some specific points. On the contrary, the other solution has a smaller NRMSE but does not reproduce all high-frequency features of the data. We argue that results of the fitting can modify the model specifications and make us reconsider the mechanisms that shape the visual response. For example, the minimum shape-error solution justifies the inclusion of a second feedback component in the model of the cone photoreceptors and horizontal cells (see reference [39] for further discussion).

In the thalamocortical system model, the transition from the waking mode to the sleep mode is initiated by the increase of the potassium leak conductance,

which triggers the hyperpolarized state of the network. During the sleep mode, the most significant changes in the intrinsic conductance values have been calculated for I_h, $I_{Na(p)}$ and I_{DK}. The interaction among these 3 currents provides a description of the up- and down-states of the slow oscillation in agreement with the study by Hill and Tononi[42]. We reproduced their simulation results by changing peak conductances of intrinsic ion channels but keeping the same network setup of the original publication. One challenge is to explore the possibility of including more parameters, in addition to peak conductances, and assess if the genetic algorithm is robust enough to provide a set of optimal parameters correlated with those computed in this work.

Another interesting issue involves calculating also the confidence interval of every single parameter wherein the model output does not deviate considerably from the optimal behavior. There are cases in which small deviations of parameters from their optimal values put the system into a different dynamical regime. Moreover, we have observed that there exist some other parameter combinations (not reported here) in our retina model that are very different from each other, and yet the output is quite similar. The reason is that we are optimizing a multi-stage model targeting the output of the whole model and many different parameter combinations of the intermediate stages can lead to a similar output. Simpler retina models, such as those based on a linear filtering stage and an integrate-and-fire output, include a fewer number of parameters and its optimization is bounded to a smaller optimal parameter range. Parameter tuning of large-scale multi-stage models could take advantage of experiments that record physiological data from every neural stage (see [26]), what would allow constraining to a greater extent the parameter range used by the automated search.

Genetic algorithm optimization has not been well explored for models of neural coding, where the fitting of large sets of parameters is an unsolved problem. In addition, neural models typically use a single fitness measure that often cannot capture all features of complex neural responses. The multi-objective optimization proposed in this work can contribute to the field of automated

parameter search of neural models.

Acknowledgments

This work has been supported by the Human Brain Project (FET project 604102), Spanish National Grants TIN2013-47069-P and TIN2015-67020-P, projects P11-TIC-7983 and P11-TIC-8120 of Junta of Andalucia (Spain), co-financed by the European Regional Development Fund (ERDF), and the Spanish Government PhD scholarship FPU13/01487. We used the supercomputer Alhambra of the University of Granada for parallel processing of the genetic algorithm optimization.

References

[1] W. Van Geit, E. De Schutter, P. Achard, Automated neuron model optimization techniques: a review, Biological cybernetics 99 (4-5) (2008) 241–251.

[2] S. Druckmann, Y. Banitt, A. Gidon, F. Schürmann, H. Markram, I. Segev, A novel multiple objective optimization framework for constraining conductance-based neuron models by experimental data, Frontiers in neuroscience 1 (1) (2007) 7.

[3] W. C. Gerken, L. Purvis, R. J. Butera, Genetic algorithm for optimization and specification of a neuron model, Neurocomputing 69 (10) (2006) 1039–1042.

[4] C. M. Weaver, S. L. Wearne, The role of action potential shape and parameter constraints in optimization of compartment models, Neurocomputing 69 (10) (2006) 1053–1057.

[5] D. Haufler, F. Morin, J. Lacaille, F. K. Skinner, Parameter estimation in single-compartment neuron models using a synchronization-based method, Neurocomputing 70 (10) (2007) 1605–1610.

[6] A. Pettinen, O. Yli-Harja, M.-L. Linne, Comparison of automated parameter estimation methods for neuronal signaling networks, Neurocomputing 69 (10) (2006) 1371–1374.

[7] A. Wohrer, P. Kornprobst, Virtual retina: a biological retina model and simulator, with contrast gain control, Journal of computational neuroscience 26 (2) (2009) 219–249.

[8] S. A. Baccus, B. P. Ölveczky, M. Manu, M. Meister, A retinal circuit that computes object motion, The Journal of Neuroscience 28 (27) (2008) 6807–6817.

[9] J. Hérault, B. Durette, Modeling visual perception for image processing, in: Computational and Ambient Intelligence, Springer, 2007, pp. 662–675.

[10] D. L. Beaudoin, B. G. Borghuis, J. B. Demb, Cellular basis for contrast gain control over the receptive field center of mammalian retinal ganglion cells, The Journal of neuroscience 27 (10) (2007) 2636–2645.

[11] N. A. Lesica, J. Jin, C. Weng, C.-I. Yeh, D. A. Butts, G. B. Stanley, J.-M. Alonso, Adaptation to stimulus contrast and correlations during natural visual stimulation, Neuron 55 (3) (2007) 479–491.

[12] C. Morillas, S. Romero, A. Martínez, F. Pelayo, L. Reyneri, M. Bongard, E. Fernández, A neuroengineering suite of computational tools for visual prostheses, Neurocomputing 70 (16) (2007) 2817–2827.

[13] R. Ferreiroa, E. Sánchez, Functional properties of a realistic model of dLGN, Neurocomputing 114 (2013) 36–44.

[14] G. T. Einevoll, H. E. Plesser, Extended difference-of-gaussians model incorporating cortical feedback for relay cells in the lateral geniculate nucleus of cat, Cognitive neurodynamics 6 (4) (2012) 307–324.

[15] N. Yousif, M. Denham, The role of cortical feedback in the generation of the temporal receptive field responses of lateral geniculate nucleus neurons:

a computational modelling study, Biological cybernetics 97 (4) (2007) 269–277.

[16] F. Hayot, D. Tranchina, Modeling corticofugal feedback and the sensitivity of lateral geniculate neurons to orientation discontinuity, Visual neuroscience 18 (06) (2001) 865–877.

[17] A. Martínez-álvarez, R. Crespo-Cano, A. Díaz-Tahoces, S. Cuenca-Asensi, J. M. F. Vicente, E. Fernández, Automatic tuning of a retina model for a cortical visual neuroprosthesis using a multi-objective optimization genetic algorithm, International Journal of Neural Systems. Accepted for publication. DOI: http://dx.doi.org/10.1142/S0129065716500210.

[18] R. Crespo-Cano, A. Martínez-Álvarez, A. Díaz-Tahoces, S. Cuenca-Asensi, J. M. Ferrández, E. Fernández, On the automatic tuning of a retina model by using a multi-objective optimization genetic algorithm, in: Artificial Computation in Biology and Medicine, Springer, 2015, pp. 108–118.

[19] Y. Ozuysal, S. A. Baccus, Linking the computational structure of variance adaptation to biophysical mechanisms, Neuron 73 (5) (2012) 1002–1015.

[20] V. Mante, V. Bonin, M. Carandini, Functional mechanisms shaping lateral geniculate responses to artificial and natural stimuli, Neuron 58 (4) (2008) 625–638.

[21] A. L. Fairhall, C. A. Burlingame, R. Narasimhan, R. A. Harris, J. L. Puchalla, M. J. Berry, Selectivity for multiple stimulus features in retinal ganglion cells, Journal of neurophysiology 96 (5) (2006) 2724–2738.

[22] H. van Hateren, A cellular and molecular model of response kinetics and adaptation in primate cones and horizontal cells, Journal of vision 5 (4) (2005) 5.

[23] J. W. Pillow, L. Paninski, V. J. Uzzell, E. P. Simoncelli, E. Chichilnisky, Prediction and decoding of retinal ganglion cell responses with a probabilistic spiking model, The Journal of Neuroscience 25 (47) (2005) 11003–11013.

[24] M. Mitchell, An introduction to genetic algorithms, MIT press, 1998.

[25] H. J. Alitto, T. G. Weyand, W. M. Usrey, Distinct properties of stimulus-evoked bursts in the lateral geniculate nucleus, The Journal of neuroscience 25 (2) (2005) 514–523.

[26] S. A. Baccus, M. Meister, Fast and slow contrast adaptation in retinal circuitry, Neuron 36 (5) (2002) 909–919.

[27] V. C. Smith, J. Pokorny, B. B. Lee, D. M. Dacey, Primate horizontal cell dynamics: an analysis of sensitivity regulation in the outer retina, Journal of Neurophysiology 85 (2) (2001) 545–558.

[28] P. Murphy, A. Sillito, Corticofugal feedback influences the generation of length tuning in the visual pathway.

[29] M. C. Vanier, J. M. Bower, A comparative survey of automated parameter-search methods for compartmental neural models, Journal of computational neuroscience 7 (2) (1999) 149–171.

[30] T. Blickle, L. Thiele, A comparison of selection schemes used in evolutionary algorithms, Evolutionary Computation 4 (4) (1996) 361–394.

[31] K. Deb, A. Pratap, S. Agarwal, T. Meyarivan, A fast and elitist multiobjective genetic algorithm: NSGA-II, Evolutionary Computation, IEEE Transactions on 6 (2) (2002) 182–197.

[32] F.-A. Fortin, F.-M. De Rainville, M.-A. Gardner, M. Parizeau, C. Gagné, DEAP: Evolutionary algorithms made easy, Journal of Machine Learning Research 13 (2012) 2171–2175.

[33] W. Gropp, E. Lusk, A. Skjellum, Using MPI: portable parallel programming with the message-passing interface, Vol. 1, MIT press, 1999.

[34] Supercomputer Alhambra of University of Granada, `http://alhambra.ugr.es`, accessed: 2016.

[35] L. D. Dalcin, R. R. Paz, P. A. Kler, A. Cosimo, Parallel distributed computing using python, Advances in Water Resources 34 (9) (2011) 1124–1139.

[36] OpenMP, `http://openmp.org/wp`, accessed: 2016.

[37] J. Granahan, J. Sweet, An evaluation of atmospheric correction techniques using the spectral similarity scale, in: Geoscience and Remote Sensing Symposium, 2001. IGARSS'01. IEEE 2001 International, Vol. 5, IEEE, 2001, pp. 2022–2024.

[38] A. Rodríguez, J. L. Nieves, E. Valero, E. Garrote, J. Hernández-Andrés, J. Romero, Modified fuzzy c-means applied to a bragg grating-based spectral imager for material clustering, in: IS&T/SPIE Electronic Imaging, International Society for Optics and Photonics, 2012, pp. 83000J–83000J.

[39] P. Martínez-Cañada, C. Morillas, B. Pino, E. Ros, F. Pelayo, A computational framework for realistic retina modeling, International Journal of Neural Systems. Accepted for publication. DOI: http://dx.doi.org/10.1142/S0129065716500301.

[40] P. Martínez-Cañada, C. Morillas, B. Pino, F. Pelayo, Towards a generic simulation tool of retina models, in: Artificial Computation in Biology and Medicine. LNCS 9107, Springer, 2015, pp. 47–57.

[41] P. Martínez-Cañada, C. Morillas, S. Romero, F. Pelayo, Modeling retina adaptation with multiobjective parameter fitting, in: Advances in Computational Intelligence. LNCS 9095, Springer, 2015, pp. 175–184.

[42] S. Hill, G. Tononi, Modeling sleep and wakefulness in the thalamocortical system, Journal of neurophysiology 93 (3) (2005) 1671–1698.

[43] J. M. Eppler, et al., NEST 2.8.0. Zenodo. (2015).
URL `http://dx.doi.org/10.5281/zenodo.32969`

[44] W. Van Geit, P. Achard, E. De Schutter, Neurofitter: a parameter tuning package for a wide range of electrophysiological neuron models, BMC Neuroscience 8 (Suppl 2) (2007) P5.